From Ziegler to Beck's column: a nonlocal approach

Noël Challamel, Attila Kocsis, Chienming Wang, Jean Lerbet

Noël Challamel · Attila Kocsis · C. M. Wang · Jean Lerbet

From Ziegler to Beck's column: a nonlocal approach

Abstract This paper is concerned with the dynamic stability of a microstructured elastic column loaded by circulatory forces. This nonconservative lattice (or discrete) problem is shown to be equivalent to the finite difference formulation of Beck's problem (cantilever column loaded by follower axial force). The lattice problem can be exactly solved from the resolution of a linear difference eigenvalue problem. The first part of the paper deals with the theoretical and numerical analyses of this discrete Beck's problem, with a particular emphasis on the flutter load sensitivity with respect to the discretization parameters, such as the number of links of the lattice. The second part of the paper is devoted to the elaboration of a nonlocal equivalent continuum that possesses similar mathematical or physical properties as compared to the original lattice model. A continualized nonlocal model is introduced first by expanding the difference operators present in the lattice equations in terms of differential operators. The length scale of the continualized nonlocal model is size independent. Next, Eringen's nonlocal phenomenological stress gradient is considered and applied at the beam scale in allowance for scale effects of the microstructured Beck column. The nonlocal Euler–Bernoulli beam model is able to capture the softening scale effect of the lattice model, even if the length scale of Eringen's model appears to be size dependent in this case. The continualized nonlocal continuum slightly differs from the Eringen's one, in the sense that the length scale affecting the static and the inertia terms differs in the deflection equation. A general parametric study illustrates the capability of each nonlocal model, the phenomenological and the continualized one, with respect to the reference lattice model. Nonlocal Beck's column is shown to be a transient medium from Ziegler's column (two-degree-of-freedom system) to the local continuous Beck's column (with an infinite degree of freedom).

N. Challamel
Laboratoire d'Ingénierie des MATériaux de Bretagne, Université de Bretagne Sud, EA 4250,
LIMATB, 56100 Lorient, France
E-mail: noel.challamel@univ-ubs.fr

A. Kocsis
Department of Structural Mechanics, Budapest University of Technology and Economics, and
Engineering Center Budapest, Robert Bosch Kft.,
Budapest 1103, Hungary
E-mail: kocsis@ep-mech.me.bme.hu

C. M. Wang
Engineering Science Programme and Department of Civil and Environmental Engineering,
National University of Singapore, Kent Ridge 119260, Singapore
E-mail: ceewcm@nus.edu.sg

J. Lerbet
Université d'Evry Val d'Essonne, UFR Sciences et Technologie, 40, rue du Pelvoux CE 1455,
91020 Evry Courcouronnes Cedex, France
E-mail: jean.lerbet@ibisc.univ-evry.fr

1

1 Introduction

Lattice systems can be considered as the reference discrete periodic media, for correctly understanding the role of microstructure in the response of a material or a structural element at a larger scale. The pioneer atomic chain model of Born and von Kármán [8], composed of concentrated masses connected by linear elastic springs, is often considered as the paradigmatic uniaxial lattice in vibrations. This uniaxial lattice, also called microstructured chain or discrete chain, has been later shown to macroscopically behave as a nonlocal continuous bar by Eringen and Kim [20] or Eringen [21]. Eringen and Kim [20] or Eringen [21] shows that the integral kernel of the nonlocal equivalent model associated with this axial lattice depended on the lattice spacing. It is worth mentioning that the model of Born and von Kármán [8] can be used for three-dimensional crystal lattice applications.

For structural mechanics applications, the reference bending lattice is the model of Hencky. Called Hencky's system [24], it comprises rigid links connected by elastic rotational springs. It was only found recently that this system behaves as a nonlocal Euler–Bernoulli beam [11,12,38], where the nonlocality may be associated with the stress gradient model of Eringen [21]. These results, valid for the bending lattice, may be also generalized to bending-shear lattices or micropolar lattice (see for instance [16,41]). The link between the microstructured bending system (Hencky's model) and some enriched Euler–Bernoulli beam models was already shown by Andrianov et al. [1] in dynamics, without direct connection to Eringen's nonlocality. The methodology for connecting the discrete system with the equivalent continuous one is based on a continualization procedure that involves expanding the difference operators present in the lattice equations with differential operators. Starting from the lattice equations of the discrete model, it is possible to define an equivalent continuum from the associated difference equations, which can be presented as an equivalent nonlocal continuum of the stress gradient type, as pioneered by Eringen [21] from a phenomenological point of view. Most of the results for this equivalence between the lattice and the equivalent nonlocal continuum have been derived for conservative elastic systems.

The aim of this paper is the generalization of this result to nonconservative elastic systems, such as circulatory systems. The structural paradigm of Beck's system composed of a cantilever elastic column loaded by a concentrated follower load has been studied in details (see [6,7,9,19,30,44]). The discrete version of this structural problem can be understood as Ziegler's column, at least for the two-degree-of-freedom system [43]. Following a continualization procedure that was previously used for the discrete Euler problem, we show that the discrete Beck system behaves as a nonlocal equivalent column (see [11] for the buckling problem under a conservative axial load; the post-buckling behaviour of this discrete column under a conservative load has been recently investigated by Challamel et al. [14] within nonlocal mechanics). In other words, there is a kind of continuous transition from the two-degree-of-freedom system (Ziegler's column—[43]) to the continuous one (Beck's column is asymptotically found for an infinite degree of freedom; [6]), possibly captured within nonlocal theories.

This paper is also related to the effect of discretization in the characterization of the stability domain of nonconservative elastic systems. Moreover, as discussed in Challamel et al. [15], there is a close connection between lattice mechanics and finite difference methods. Hencky's system can be considered as the physical representation of the finite difference method applied to a continuous beam problem [35]. Leipholz [29], Sugiyama et al. [36,37], El Naschie and Al-Athel [17,18] investigated nonconservative problems with distributed axial forces by the finite difference method (or the discrete element method). El Naschie and Al-Athel [17,18] used a discrete element method (equivalent to Hencky's bar-chain system) under distributed axial follower load with a modified clamped boundary condition based on a clamped rotational stiffness larger than two times the internal rotational stiffness. This approach can be shown to be equivalent to the finite difference method, except eventually for the modelling of the clamped section. More specifically with respect to the present study devoted to Beck's column, Sugiyama et al. [36] also specifically investigated the Beck's column by the equivalent finite difference method. El Naschie and Al-Athel [18] studied a massless Beck's column with a concentrated tip mass, using Hencky's system. More recently, the specific effect of discretization of columns in the presence of follower loads has been numerically handled by Gasparini et al. [23] without any theoretical correspondence with nonlocal theories. Luongo and D'Annibale [31] investigated the destabilizing role of damping in discrete and continuous systems, without focusing specifically on the possible connection

between the discrete system and the continuous one. Awrejcewicz et al. [5] used the finite difference method for highlighting chaos in the vibration of curvilinear Euler–Bernoulli beams.

The nonlocal Beck's problem has been already investigated by Xiang et al. [40] from an Eringen's nonlocal beam model. Xiang et al. [40] showed the softening effect of the small length terms on the flutter load. Lazopoulos and Lazopoulos [27] investigated the flutter behaviour of a gradient elasticity Beck column and highlighted the stiffening effect of the small length scale terms. More recently, Atanackovic et al. [4] investigated the flutter load of nonlocal viscoelastic beam on elastic foundation. They showed that the flutter load is affected by the small length scale terms (which tend to reduce the flutter load), even if the flutter load surprisingly does not depend on the foundation modulus. This paradoxical insensitivity is known as the Hermann–Smith paradox, which can be removed by introducing the viscoelastic dependence of the beam. The nonlocality considered by Xiang et al. [40] or by Atanackovic et al. [4], based on Eringen's differential law, was assumed from a phenomenological nonlocal model. However, the source of nonlocality from the discrete analogy of the structural system was not discussed in these studies. This paper focuses on the definition of a nonlocal beam model that is valid for both conservative and nonconservative loadings and is defined from a microstructured or a lattice model.

2 Review of Beck's column

In this part, the review of Beck's problem is presented. As will be shown later in the paper, equations of local Beck's column, discrete Beck's column or nonlocal Beck's column have mathematical similarities. The flutter load of each system is computed for each model from the calculation of a four-dimensional determinant. Beck's column is an Euler–Bernoulli beam clamped at one end and free at the other end. The free end (the tip) is subjected to a follower force: a compressive force P whose line of action is always tangential to the slope of the deformed column at the tip. By assuming small displacements, initially straight column, linear elasticity, and neglecting the rotary inertia, the partial differential equation of Beck's problem is given by [6]:

$$EI\partial_x^4 \widehat{w}(x,t) + P\partial_x^2 \widehat{w}(x,t) + \mu \ddot{\widehat{w}}(x,t) = 0 \tag{1}$$

Here $\widehat{w}(x,t)$ denotes the deflection of the column, EI is its flexural rigidity, P the compressive follower force, μ the mass per unit length, the superdot denotes differentiation with respect to time t, and the symbol

$$\partial_x = \frac{\partial}{\partial x} \tag{2}$$

By using the dimensionless coordinate $\varsigma = x/L$, and introducing the deflection as the function of ς, i.e. $w(\varsigma,t) = \widehat{w}(L\varsigma,t)$, in Eq. (1), we have

$$\frac{EI}{L^4}w^{(4)}(\varsigma,t) + \frac{P}{L^2}w''(\varsigma,t) + \mu \ddot{w}(\varsigma,t) = 0 \tag{3}$$

Here the prime denotes differentiation with respect to ς. The solution for Eq. (3) is assumed in the following separable form:

$$w(\varsigma,t) = w(\varsigma) \cdot e^{j\omega \cdot t}$$

where $j = \sqrt{-1}$ is the imaginary unit and ω the circular frequency. If ω is real, then the vibration of the column is stable (in the *Lyapunov* sense). In view of the separable form of deflection, Eq. (3) may be re-written as an ordinary differential equation

$$w^{(4)} + \Lambda w'' - \Omega^2 w = 0 \tag{4}$$

where the load and frequency parameters, Λ and Ω, are defined as

$$\Lambda = \frac{PL^2}{EI} \quad \text{and} \quad \Omega^2 = \frac{\omega^2 L^4 \mu}{EI} \tag{5}$$

The solution for Eq. (4) is:

$$w(\varsigma) = A\cosh(\widehat{s}_1\varsigma) + B\sinh(\widehat{s}_1\varsigma) + C\cos(\widehat{s}_2\varsigma) + D\sin(\widehat{s}_2\varsigma) \tag{6}$$
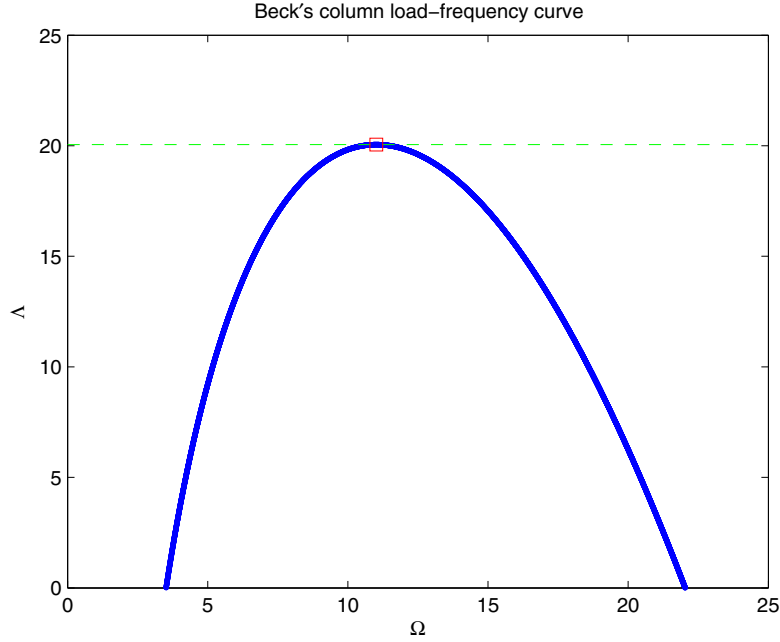
3

Fig. 1 Load–frequency *curve* of Beck's column. The flutter load–flutter frequency pair is denoted by a box. *Dashed line* shows the flutter load level

where

$$\widehat{s}_1 = \sqrt{\sqrt{\frac{\Lambda^2}{4} + \Omega^2} - \frac{\Lambda}{2}} \quad \text{and} \quad \widehat{s}_2 = \sqrt{\sqrt{\frac{\Lambda^2}{4} + \Omega^2} + \frac{\Lambda}{2}} \tag{7}$$

The boundary conditions of the column are:

$$w(0) = 0, \, w'(0) = 0 \quad \text{and} \quad w''(1) = 0, \, w'''(1) = 0 \tag{8}$$

By substituting Eq. (6) into the boundary conditions given by Eq. (8), one obtains an eigenvalue problem. For a nontrivial solution, the determinant of the frequency matrix has to vanish, i.e.

$$\begin{vmatrix} 1 & 0 & 1 & 0 \\ 0 & \widehat{s}_1 & 0 & \widehat{s}_2 \\ \widehat{s}_1^2 \cosh(\widehat{s}_1) & \widehat{s}_1^2 \sinh(\widehat{s}_1) & -\widehat{s}_2^2 \cos(\widehat{s}_2) & -\widehat{s}_2^2 \sin(\widehat{s}_2) \\ \widehat{s}_1^3 \sinh(\widehat{s}_1) & \widehat{s}_1^3 \cosh(\widehat{s}_1) & \widehat{s}_2^3 \sin(\widehat{s}_2) & -\widehat{s}_2^3 \cos(\widehat{s}_2) \end{vmatrix} = 0$$

The above characteristic equation is a highly nonlinear equation. One may solve this characteristic equation for Λ and Ω by using the shooting method, assuming a real frequency parameter Ω. Solutions are plotted in Fig. 1 in the domain of $\Lambda \in [0, 25]$, $\Omega \in [0, 25]$. Two roots can be seen for the unloaded column, i.e. for $\Lambda = 0$, which are the first two nondimensional natural frequency parameters of the clamped column. By increasing the load, these two roots get closer to each other and coincide at the flutter load parameter $\Lambda_{\text{flut}}^{\text{Beck}} = 20.051$ and frequency parameter $\Omega_{\text{flut}}^{\text{Beck}} = 11.016$ [6]. The two roots become complex conjugate at the flutter load level in which Beck's column undergoes a dynamic loss of stability.

3 The discrete Beck's problem

The discrete Beck's problem is shown in Fig. 2. This microstructured elastic system comprises n cells, as it is a discretized beam of length L composed of n repetitive cells of size a. In other words, the total length of
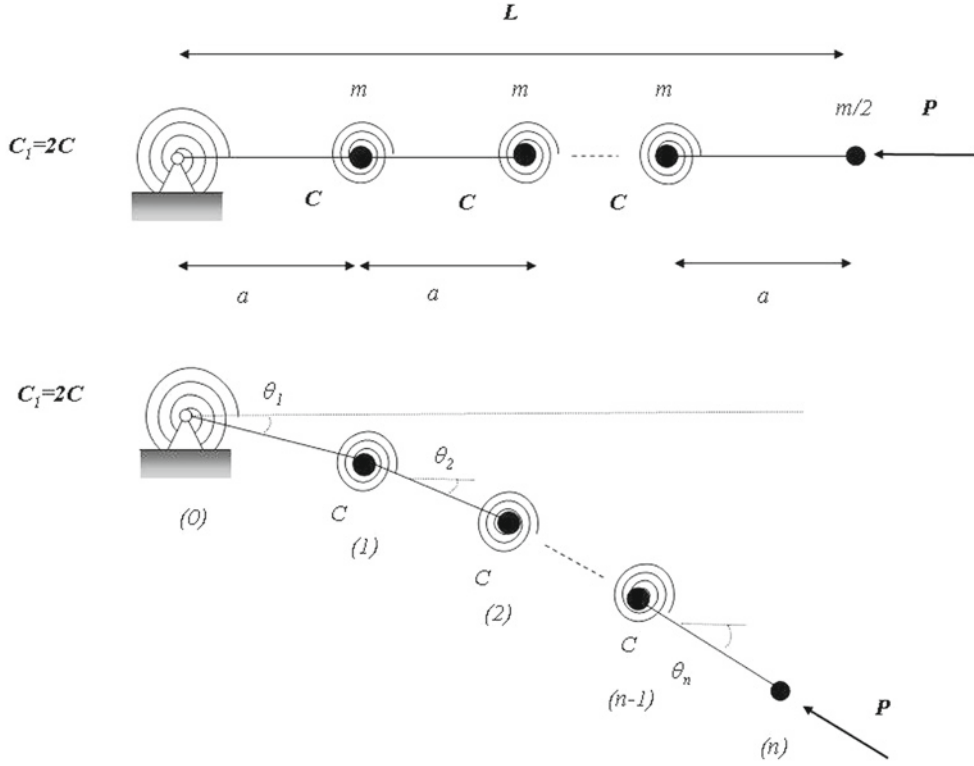
Fig. 2 Discrete Beck's problem

the structure L is equal to $L = n \times a$, i.e. the number of repetitive cells multiplied by the size of each cell. The cells are connected by frictionless hinges of mass m and coupled by elastic rotational springs of stiffness C. The correspondence between the discrete and the continuous systems yields $C = EI/a$ for the spring stiffness and $m = \mu a$ for the mass, where EI is the bending stiffness and μ is the mass per unit length of the continuum. The end inertial mass is half of that in the middle in order to maintain the total mass conservation, $n \times m = \mu L$. One end of the beam is attached to the ground and equipped with a rotational spring of stiffness C_1. The other (free) end is loaded by a follower force denoted by P. The stability of the discrete system under the nonconservative follower force is studied with the dynamic method under the assumption of small displacements. Note that the equilibrium method cannot capture dynamic loss of stability of nonconservative systems, as it was demonstrated on similar discrete models by Kocsis et al. [25], Kocsis [26].

In order to obtain the governing equations of the system, D'Alembert's principle along with the principle of virtual displacements is utilized [22]. The virtual work done by the moments in the spring on a virtual displacement system is given by

$$\delta W_{\text{int}} = C_1 \frac{w_1(t)}{a} \frac{\delta w_1}{a} + C \sum_{i=1}^{n} \left(\frac{w_{i+1}(t) - 2w_i(t) + w_{i-1}(t)}{a} \right) \left(\frac{\delta w_{i+1} - 2\delta w_i + \delta w_{i-1}}{a} \right) \tag{9}$$

Here $w_i(t) = \widehat{w}(x = ia, t)$ is the vertical translation of node i as the function of time, δw_i is an arbitrary virtual displacement of node i, and $C_1 = 2C$ is the rotational spring stiffness at the clamped end.

The virtual work done by the follower force is:

$$\delta W_{\text{ext}} = Pa \sum_{i=1}^{n} \left(\frac{w_i(t) - w_{i-1}(t)}{a} \right) \left(\frac{\delta w_i - \delta w_{i-1}}{a} \right) - P \left(\frac{w_n(t) - w_{n-1}(t)}{a} \right) \delta w_n \tag{10}$$

The work done by the fictitious inertial force on a virtual displacement system is:

$$\delta W_f = -m \sum_{i=1}^{n-1} \ddot{w}_i(t) \delta w_i - \frac{m}{2} \ddot{w}_n(t) \delta w_n \tag{11}$$

5

The total virtual work $\delta W = \delta W_{\text{int}} - \delta W_{\text{ext}} - \delta W_f$ is zero for *any* virtual displacement system. It yields:

$$EI\frac{w_{i+2}(t) - 4w_{i+1}(t) + 6w_i(t) - 4w_{i-1}(t) + w_{i-2}(t)}{a^4} + P\frac{w_{i+1}(t) - 2w_i(t) + w_{i-1}(t)}{a^2} + \mu\ddot{w}_i(t) = 0 \tag{12}$$

for $i = 1 \ldots n - 1$, with the following boundary conditions prescribed at the clamped end:

$$w_0 = 0 \quad \text{and} \quad w_{-1} = w_1 \tag{13}$$

The far-end boundary conditions of this non-self-adjoined problem are obtained from the virtual work theorem for node $i = n$:

$$w_{n+1} - 2w_n + w_{n-1} = 0 \quad \text{and} \quad w_{n+1} - 3(w_n - w_{n-1}) - w_{n-2} + \frac{\Omega}{2n^4}w_n = 0 \tag{14}$$

Note that the last condition (free-end boundary condition) reduces to the one obtained by Leckie and Lindberg [28] for a free vibration problem with the finite difference method.

One can immediately recognize that Eq. (12) is the finite difference version of Eq. (1). Hence, the discrete, microstructured system is mathematically equivalent to the finite difference format of the so-called local continuum (see the remark of [35], and the debate about the physical interest of Hencky's bar-chain compared to the "abstract" numerical-based finite difference method; see more recently [11,12]). The discrete Beck's problem, under investigation, is nothing else but the finite difference formulation of the Beck's continuous problem governed by Eq. (1):

$$EI\delta_0^4\widehat{w} + P\delta_0^2\widehat{w} + \mu\ddot{\widehat{w}} = 0 \tag{15}$$

where

$$\delta_0^4\widehat{w} = \frac{w_{i+2}(t) - 4w_{i+1}(t) + 6w_i(t) - 4w_{i-1}(t) + w_{i-2}(t)}{a^4} \quad \text{and} \quad \delta_0^2\widehat{w} = \frac{w_{i+1}(t) - 2w_i(t) + w_{i-1}(t)}{a^2}$$

Here δ_0 is the first-order central difference. This linear finite difference equation can be solved exactly. First, the nodal displacement is written in the form of

$$w_i(t) = w_i \cdot e^{j\omega \cdot t} \tag{16}$$

with j being the imaginary unit, ω being the vibration frequency of the beam, and w_i being the nodal displacement amplitude. It is substituted in Eq. (15), leading to the time-independent difference equation:

$$H_i + \frac{\Lambda}{n^2}G_i - \frac{\Omega^2}{n^4}w_i = 0 \quad (i \in [1, n-1]) \tag{17}$$

where

$$H_i = w_{i+2} - 4w_{i+1} + 6w_i - 4w_{i-1} + w_{i-2} \tag{18a}$$
$$G_i = w_{i+1} - 2w_i + w_{i-1} \tag{18b}$$

and Λ and Ω are given by Eq. (5). Now Λ and Ω denote nondimensional load and vibration frequency parameters, respectively, of the microstructured model. The boundary conditions for Eq. (17) are given by Eqs. (13) and (14).

Next, the fourth-order finite difference equation is exactly solved, following the procedure described in Santoro and Elishakoff [34], Challamel et al. [11–13] or Zhang et al. [42]. The discrete displacement field of the microstructured beam model can be assumed as

$$w_i = B\gamma^i \tag{19}$$

where B is a constant. Therefore, Eq. (17) may be written as

$$\Gamma^2 - (4 - A_1)\Gamma + 4 - 2A_1 + A_2 = 0 \tag{20}$$

where

$$\Gamma = \gamma + \frac{1}{\gamma}, \quad A_1 = \frac{\Lambda}{n^2}, \quad A_2 = -\frac{\Omega}{n^4}.$$

By solving Eq. (20), one obtains

$$\Gamma_{1,2} = 2 - \frac{\Lambda}{2n^2} \mp \frac{\sqrt{\Lambda^2 + 4\Omega}}{2n^2} \tag{21}$$

Therefore

$$\gamma_{1,2} = 1 - \frac{1}{4n^2}\left[\Lambda + \sqrt{\Lambda^2 + 4\Omega}\right] \mp j\sqrt{1 - \left[1 - \frac{\Lambda}{4n^2} - \frac{1}{4n^2}\sqrt{\Lambda^2 + 4\Omega}\right]^2} \tag{22a}$$

$$\gamma_{3,4} = 1 - \frac{1}{4n^2}\left[\Lambda - \sqrt{\Lambda^2 + 4\Omega}\right] \mp \sqrt{\left[1 - \frac{\Lambda}{4n^2} + \frac{1}{4n^2}\sqrt{\Lambda^2 + 4\Omega}\right]^2 - 1} \tag{22b}$$

where $j = \sqrt{-1}$ is the imaginary unit. From Eq. (22), one can assume that

$$\cos\phi = 1 - \frac{\Lambda}{4n^2} - \frac{1}{4n^2}\sqrt{\Lambda^2 + 4\Omega} \tag{23a}$$

$$\cosh\vartheta = 1 - \frac{\Lambda}{4n^2} + \frac{1}{4n^2}\sqrt{\Lambda^2 + 4\Omega} \tag{23b}$$

Therefore

$$\gamma_{1,2} = \cos\phi \mp j \cdot \sin\phi \tag{24a}$$
$$\gamma_{3,4} = \cosh\vartheta \mp \sinh\vartheta \tag{24b}$$

In view of Eq. (24), the general solution for w_i can be represented as

$$w_i = A_1 \cos(i\phi) + A_2 \sin(i\phi) + A_3 \cosh(i\vartheta) + A_4 \sinh(i\vartheta) \tag{25}$$

In view of the boundary conditions of Eqs. (13) and (14), the load–frequency relationship can be obtained from the following characteristic equation:

$$\begin{vmatrix} 1 & 0 & 1 & 0 \\ 0 & \sin\phi & 0 & \sinh\vartheta \\ \cos(n\phi)(\cos\phi - 1) & \sin(n\phi)(\cos\phi - 1) & \cosh(n\vartheta)(\cosh\vartheta - 1) & \sinh(n\vartheta)(\cosh\vartheta - 1) \\ F_1 & F_2 & F_3 & F_4 \end{vmatrix} = 0 \tag{26}$$

where

$$F_1 = \left[\frac{\Omega}{2n^4} - 2(\cos\phi - 1)^2\right]\cos(n\phi) - [2(\cos\phi - 1)]\sin(n\phi)\sin\phi \tag{27a}$$

$$F_2 = \left[\frac{\Omega}{2n^4} - 2(\cos\phi - 1)^2\right]\sin(n\phi) + [2(\cos\phi - 1)]\cos(n\phi)\sin\phi \tag{27b}$$

$$F_3 = (4 - 2\cosh\vartheta)\cosh(n\vartheta)\cosh\vartheta - (2 - 2\cosh\vartheta)\sinh(n\vartheta)\sinh\vartheta - \left(2 - \frac{\Omega}{2n^4}\right)\cosh(n\vartheta) \tag{27c}$$

$$F_4 = (4 - 2\cosh\vartheta)\sinh(n\vartheta)\cosh\vartheta - (2 - 2\cosh\vartheta)\cosh(n\vartheta)\sinh\vartheta - \left(2 - \frac{\Omega}{2n^4}\right)\sinh(n\vartheta) \tag{27d}$$

The flutter load, $\Lambda_{flut}^{\text{disc},n}$, and flutter frequency, $\Omega_{flut}^{\text{disc},n}$, can be computed from Eq. (26) for a given number of cells n. The roots of Eq. (26) for zero load $\Lambda = 0$ yield the natural vibration frequencies of the microstructured model.

The flutter load for the two-degree-of-freedom Ziegler's type system, $n = 2$, is $\Lambda_{flut}^{\text{disc},2} = 8$. This value can be numerically obtained from the load–frequency relationship Eq. (26), or analytically obtained, as detailed
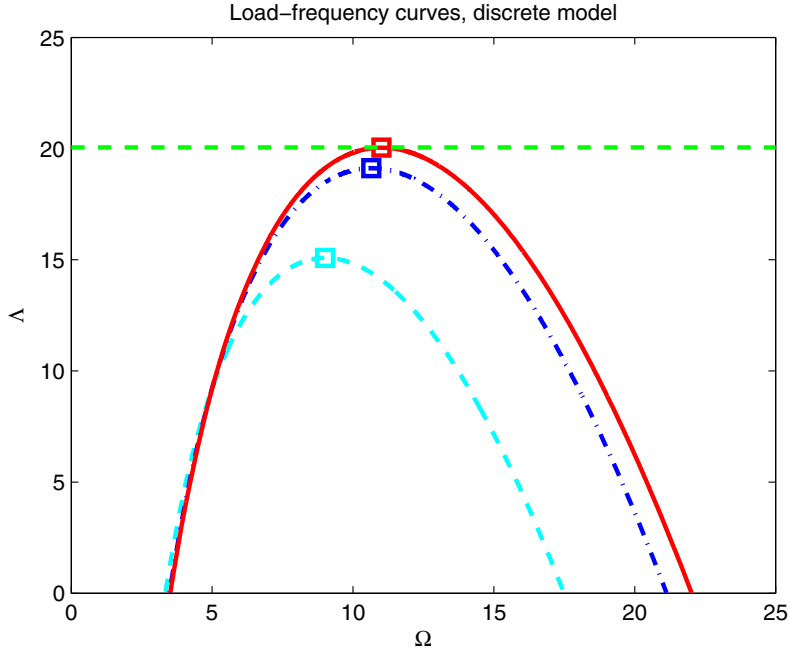
Fig. 3 Comparison of load–frequency *curve* of the microstructured model for different values of *n*; *n* = 4 (*cyan dashed line*); *n* = 10 (*blue dash-dot line*) and *n* = 100 (*red solid line*). The flutter load–flutter frequency pair is denoted by a box. *Horizontal dashed line* shows the flutter load level of the local continuum (Beck's solution). (Color figure online)
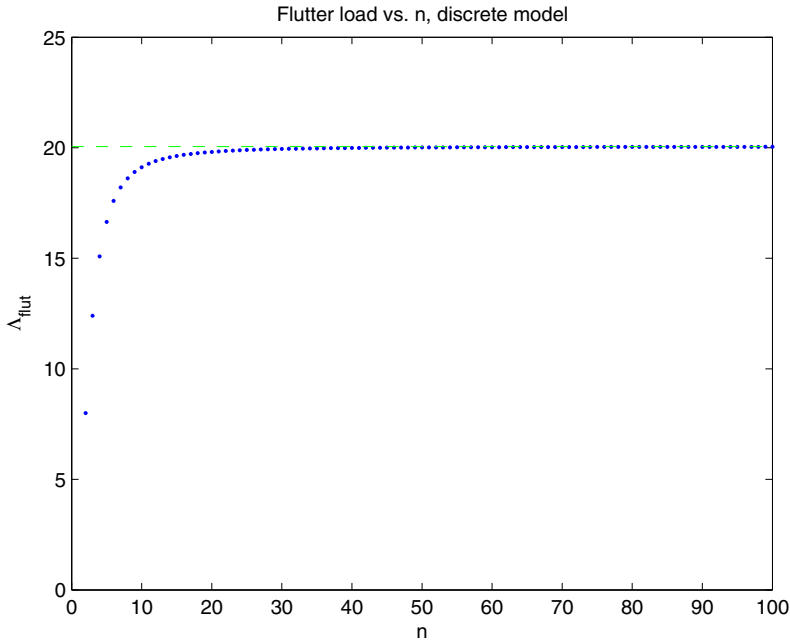

Fig. 4 Flutter load of the discrete model versus the number of cells *n*. *Dashed line* shows the flutter load level of Beck's column

in "Appendix 1". A closed-form equation of the flutter load can be also obtained for $n = 3$, leading to $\Lambda_{\text{flut}}^{\text{disc},3} \approx 12.4023$, as shown in "Appendix 2". The nondimensional flutter load parameter increases with the number of cells *n*. For larger values of *n*, the flutter load and the flutter frequency parameters can be obtained numerically, by using the shooting method.

Figure 3 shows the load–frequency curve, $f(\Lambda, \Omega) = 0$, for different values of *n* cells in the domain of $\Lambda \in [0, 25]$, $\Omega \in [0, 25]$. The flutter load and flutter frequency parameters are: $\Lambda_{\text{flut}}^{\text{disc},4} = 15.0834$ and
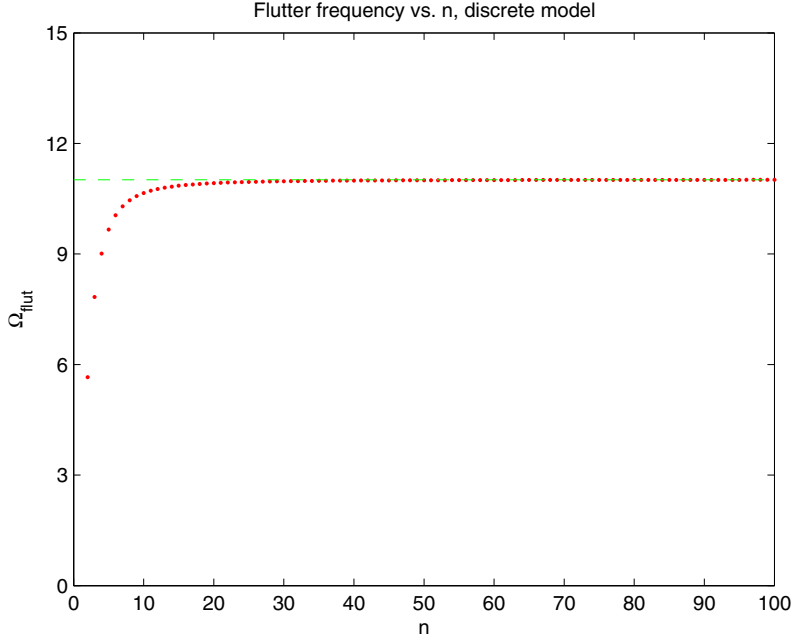
8

Fig. 5 Flutter frequency of the discrete model versus the number of cells n. *Dashed line* shows the flutter frequency of Beck's column

$\Omega_{\text{flut}}^{\text{disc},4} = 9.011$, respectively, for $n = 4$. The first natural frequency is $\Omega_{\text{free}}^{\text{disc},4} = 3.342$. The same curve is plotted for $n = 10$ cells. The flutter load and flutter frequency parameters in this case are: $\Lambda_{\text{flut}}^{\text{disc},10} = 19.1175$ and $\Omega_{\text{flut}}^{\text{disc},10} = 10.653$, respectively. The first natural frequency is $\Omega_{\text{free}}^{\text{disc},10} = 3.487$. The case of $n = 100$ cells almost corresponds to the so-called local Beck's column (without scale effects). The flutter load and flutter frequency parameters in this case are: $\Lambda_{\text{flut}}^{\text{disc},100} = 20.0413$ and $\Omega_{\text{flut}}^{\text{disc},100} = 11.012$, respectively. The first natural frequency is $\Omega_{\text{free}}^{\text{disc},100} = 3.516$. Figure 4 shows the flutter load versus the number of cells n. Figure 5 shows the flutter frequency versus the number of cells n. All of these values tend to *Beck*'s solution as n increases. As classically observed for these lattice-type systems (see [12]), the microstructure effect tends to soften the lattice system when compared to the local continuous one. This softening effect is also confirmed here for the flutter load dependency to the number of cells n.

4 A nonlocal Beck's problem by continualization

The discrete equations are extended to an equivalent continuum via a continualization method. The following relation between the discrete and the equivalent continuous system $w_i = \widehat{w}(x = ia)$ holds for a sufficiently smooth deflection function:

$$\widehat{w}(x + a) = \sum_{k=0}^{\infty} \frac{a^k \partial_x^k}{k!} \widehat{w}(x) = e^{a\partial_x} \widehat{w}(x) \tag{28}$$

with ∂_x given by Eq. (2). One can calculate the generalized Laplacian $\Delta_0 = \delta_0^2$ and its square part $\Delta_0^2 = \delta_0^4$:

$$\delta_0^2 = \frac{4}{a^2} \sinh^2\left(\frac{a}{2}\partial_x\right), \quad \delta_0^4 = \frac{16}{a^4} \sinh^4\left(\frac{a}{2}\partial_x\right) \tag{29}$$

The pseudo-differential Laplacian operator can be efficiently approximated by the Padé's approximant (see, for instance [2,32,33,39] or [3] for axial wave applications):

$$\frac{4}{a^2} \sinh^2\left(\frac{a}{2}\partial_x\right) = \frac{\partial_x^2}{1 - l_c^2 \partial_x^2} + \dots \quad \text{with } l_c^2 = \frac{a^2}{12} \tag{30}$$

9

Equation (15) can then be approximated by the continuous analogy:

$$EI \frac{\partial_x^4 \widehat{w}(x)}{\left(1 - l_c^2 \partial_x^2\right)^2} + P \frac{\partial_x^2 \widehat{w}(x)}{\left(1 - l_c^2 \partial_x^2\right)} - \mu\omega^2 \widehat{w}(x) = 0 \tag{31}$$

or equivalently, if $\mu\omega^2 l_c^4 \partial_x^4 \widehat{w}(x)$ is neglected:

$$\left(EI - Pl_c^2\right) \partial_x^4 \widehat{w}(x) + \left(P + 2\mu\omega^2 l_c^2\right) \partial_x^2 \widehat{w}(x) - \mu\omega^2 \widehat{w}(x) = 0 \quad \text{with } l_c^2 = \frac{a^2}{12} \tag{32}$$

By using $\varsigma = x/L$ and $w(\varsigma) = \widehat{w}(L\varsigma)$, Eq. (32) may be written in the following form:

$$\frac{\left(EI - Pl_c^2\right)}{L^4} w^{(4)} + \frac{\left(P + 2\mu\omega^2 l_c^2\right)}{L^2} w'' - \mu\omega^2 w = 0 \quad \text{with } l_c^2 = \frac{L^2}{12n^2}$$

By introducing the parameters (p, q) defined as

$$p = \frac{\Lambda + \frac{\Omega^2}{6n^2}}{1 - \frac{\Lambda}{12n^2}} \quad \text{and} \quad q^2 = \frac{\Omega^2}{1 - \frac{\Lambda}{12n^2}} \tag{33}$$

the governing equation of the nonlocal continuum associated with the discrete Beck's problem can be compactly expressed as

$$w^{(4)} + pw'' - q^2 w = 0 \tag{34}$$

Note that p and q tend to Λ and Ω, respectively, and Eq. (34) coincides with Eq. (4) if $n \to \infty$.

The boundary conditions of the nonlocal continuum are given at the clamped end by $\widehat{w}(0) = 0$ and $\widehat{w}(-a) = \widehat{w}(a)$, which can be presented with $w(\varsigma)$ as:

$$w(0) = 0 \quad \text{and} \quad w\left(-\frac{1}{n}\right) = w\left(\frac{1}{n}\right) \tag{35}$$

These equivalent kinematic boundary conditions have also been considered by Challamel et al. [12] and are slightly different from a fully constrained clamped section. Now, the following free-end boundary conditions may be obtained from variational principles (see [10] as well as [13] for a discussion on the free end conditions of conservative nonlocal Euler–Bernoulli beam models):

$$\left[EI\widehat{w}'' \delta \widehat{w}'\right]_0^L = 0 \quad \text{and} \quad \left[\left(EI\widehat{w}''' + 2\mu l_c^2 \omega^2 \widehat{w}'\right)\delta\widehat{w}\right]_0^L = 0 \tag{36}$$

It is assumed that the boundary conditions are not affected at the free end by the presence of the follower load, leading to:

$$EI\widehat{w}''(L) = 0 \quad \text{and} \quad EI\widehat{w}'''(L) + 2\mu l_c^2 \omega^2 \widehat{w}'(L) = 0 \tag{37}$$

It can be presented with $w(\varsigma)$ as:

$$w''(1) = 0 \quad \text{and} \quad w'''(1) + rw'(1) = 0 \quad \text{with } r = \frac{\Omega^2}{6n^2} \tag{38}$$

The general solution of Eq. (34) is:

$$w(\varsigma) = A\cosh(s_1 \varsigma) + B\sinh(s_1 \varsigma) + C\cos(s_2 \varsigma) + D\sin(s_2 \varsigma)$$

where

$$s_1 = \sqrt{\sqrt{\frac{p^2}{4} + q^2} - \frac{p}{2}} \quad \text{and} \quad s_2 = \sqrt{\sqrt{\frac{p^2}{4} + q^2} + \frac{p}{2}} \tag{39}$$

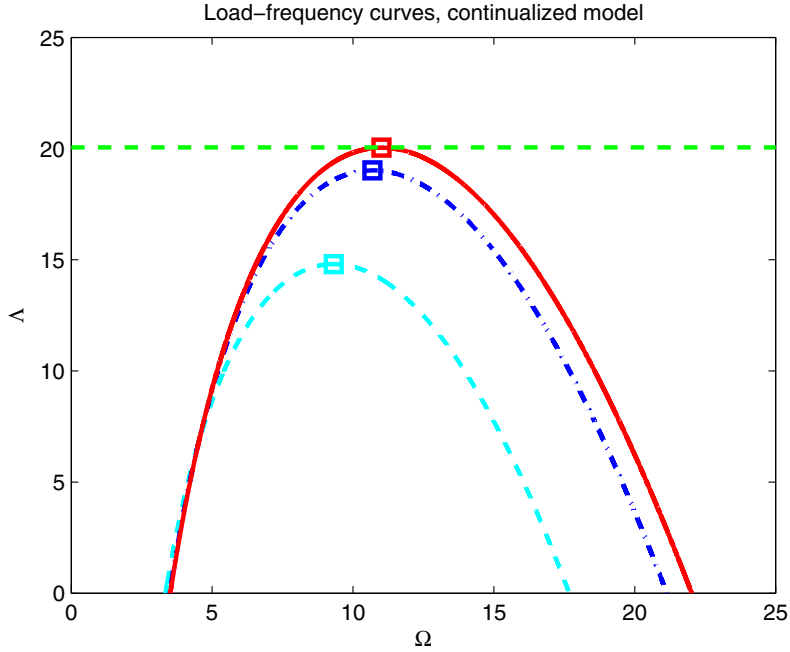Note that Eq. (39) yields Eq. (7) as $n \to \infty$.

Fig. 6 Comparison of load–frequency *curve* of the continualized model for different values of n; $n = 4$ (*cyan dashed line*); $n = 10$ (*blue dash-dot line*); and $n = 100$ (*red solid line*). The flutter load–flutter frequency pair is denoted by a box. *Horizontal dashed line* shows Beck's flutter load. (Color figure online)

In view of the boundary conditions Eq. (35) and Eq. (38), one obtains the determinant equation for the load–frequency relationship of the equivalent continuum:

$$
\begin{vmatrix}
1 & 0 & 1 & 0 \\
0 & \sinh(s_1/n) & 0 & \sin(s_2/n) \\
s_1^2 \cosh(s_1) & s_1^2 \sinh(s_1) & -s_2^2 \cos(s_2) & -s_2^2 \sin(s_2) \\
(s_1^3 + s_1 r) \sinh(s_1) & (s_1^3 + s_1 r) \cosh(s_1) & (s_2^3 - s_2 r) \sin(s_2) & -(s_2^3 - s_2 r) \cos(s_2)
\end{vmatrix} = 0 \quad (40)
$$

Eq. (40) can also be presented equivalently as:

$$
\begin{aligned}
& s_2^3 (s_2^2 - r) \sinh(s_1/n) + s_1^3 (s_1^2 + r) \sin(s_2/n) \\
& + s_1 s_2 \sin(s_2) \sinh(s_1) \left[s_1 (s_2^2 - r) \sin(s_2/n) - s_2 (s_1^2 + r) \sinh(s_1/n) \right] \\
& + s_1 s_2 \cos(s_2) \cosh(s_1) \left[s_2 (s_1^2 + r) \sin(s_2/n) + s_1 (s_2^2 - r) \sinh(s_1/n) \right] = 0 \quad (41)
\end{aligned}
$$

Figure 6 shows the load–frequency curve, $f(\Lambda, \Omega) = 0$, for $n = 4$, $n = 10$ and $n = 100$ in the domain of $\Lambda \in [0, 25]$, $\Omega \in [0, 25]$. The flutter load and flutter frequency parameters are: $\Lambda_{\text{flut}}^{\text{cont},4} = 14.8052$ and $\Omega_{\text{flut}}^{\text{cont},4} = 9.316$, respectively. The first natural frequency parameter is $\Omega_{\text{free}}^{\text{cont},4} = 3.344$. The same curve is plotted for $n = 10$. The flutter load and flutter frequency parameters are: $\Lambda_{\text{flut}}^{\text{cont},10} = 19.0209$ and $\Omega_{\text{flut}}^{\text{cont},10} = 10.698$, respectively. The first natural frequency parameter is $\Omega_{\text{free}}^{\text{cont},10} = 3.487$. The case of $n = 100$ is very close to the local Beck's column. The flutter load and flutter frequency parameters in this case are: $\Lambda_{\text{flut}}^{\text{cont},100} = 20.0402$ and $\Omega_{\text{flut}}^{\text{cont},100} = 11.012$, respectively. The first natural frequency parameter is $\Omega_{\text{free}}^{\text{cont},100} = 3.516$.

Figure 7 shows the flutter load parameter versus n in the case of the continualized model. Figure 8 shows the flutter frequency parameter versus n. All these values tend to Beck's solution as n increases. The response of this continualized nonlocal model is very similar to the one of the discrete Beck's column; especially, the softening effect induced by the microstructure is observed, as already detailed for the lattice reference system.
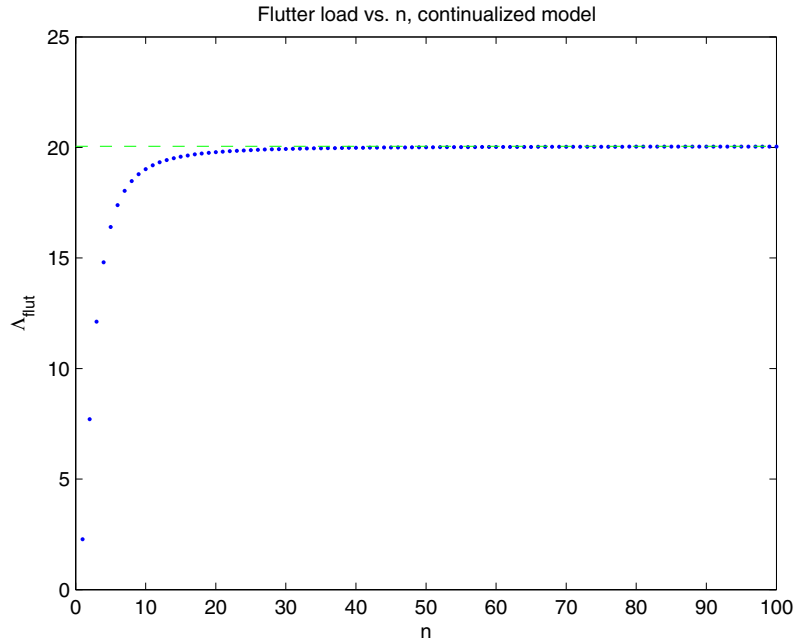
Fig. 7 Flutter load parameter of the continualized model versus *n*. *Dashed line* shows the flutter load of Beck's column
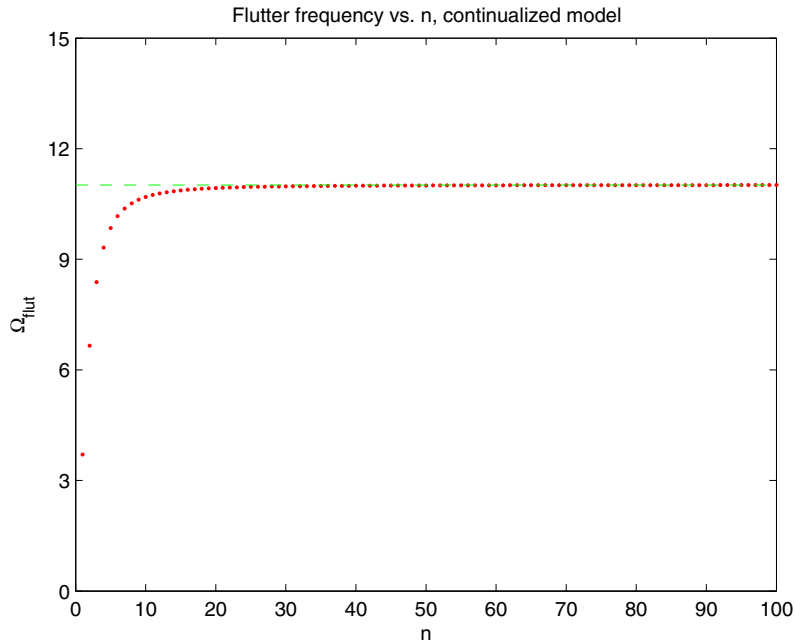

Fig. 8 Flutter frequency parameter of the continualized model versus *n*. *Dashed line* shows the flutter frequency of Beck's column

5 Eringen's nonlocal Beck's problem

Xiang et al. [40] investigated the stability of a nonlocal elastic column under a follower force, which can be referred as the nonlocal Beck's problem, where the bending moment–curvature follows the Eringen's nonlocal law (see [21] for the nonlocal stress–strain differential equation):

$$M - l_c^2 \partial_x^2 M = EI \partial_x^2 \widehat{w} \tag{42}$$

12

As shown by Xiang et al. [40], the ordinary differential equation of the deflection for investigating the dynamic stability of the nonlocal Beck's column is:

$$\left(EI - Pl_c^2\right) \partial_x^4 \widehat{w} + \left(P + \mu\omega^2 l_c^2\right) \partial_x^2 \widehat{w} - \mu\omega^2 \widehat{w} = 0 \tag{43}$$

Note at this stage the fundamental difference between Eq. (32) and Eq. (43). This shows that the continualization of the discrete problem is different in nature from the nonlocal Eringen's column. This phenomenon has been carefully analysed in Challamel et al. [12,13], who showed that the source of discrepancy was linked to the continualization of the equilibrium equations. It is assumed in this present model that the length scale is fixed, say $l_c^2 = a^2/12$ or $l_c^2 = a^2/6$. However, it would be also possible to fit the nonlocal model with respect to the lattice one with a variable size-dependent length scale parameter.

By using ς and $w(\varsigma) = \widehat{w}(L\varsigma)$, the governing equation of the nonlocal continuum associated with the discrete Beck's problem has a similar fourth-order form as Eq. (34), i.e.

$$w^{(4)} + \widetilde{p}w'' - \widetilde{q}^2 w = 0 \tag{44}$$

The modified nonlocal parameters $(\widetilde{p}, \widetilde{q})$ are:

$$\widetilde{p} = \frac{\Lambda + \frac{\Omega^2}{12n^2}}{1 - \frac{\Lambda}{12n^2}} \neq p \quad \text{and} \quad \widetilde{q}^2 = \frac{\Omega^2}{1 - \frac{\Lambda}{12n^2}} = q^2 \tag{45}$$

Note that Eqs. (44) and (45) are the same as Eqs. (4) and (7), respectively, in the limit $n \to \infty$.

The boundary conditions of the Euler–Bernoulli nonlocal beam model are (see [40]):

$$w(0) = 0, \quad w'(0) = 0, \quad w''(1) + \widetilde{r}w(1) = 0 \quad \text{and} \quad w'''(1) + \widetilde{r}w'(1) = 0 \quad \text{with} \quad \widetilde{r} = \frac{\frac{\Omega^2}{12n^2}}{1 - \frac{\Lambda}{12n^2}} \tag{46}$$

The general solution of Eq. (44) can be written as:

$$w(\varsigma) = A \cosh(\widetilde{s}_1\varsigma) + B \sinh(\widetilde{s}_1\varsigma) + C \cos(\widetilde{s}_2\varsigma) + D \sin(\widetilde{s}_2\varsigma)$$

where

$$\widetilde{s}_1 = \sqrt{\sqrt{\frac{\widetilde{p}^2}{4} + \widetilde{q}^2} - \frac{\widetilde{p}}{2}} \quad \text{and} \quad \widetilde{s}_2 = \sqrt{\sqrt{\frac{\widetilde{p}^2}{4} + \widetilde{q}^2} + \frac{\widetilde{p}}{2}} \tag{47}$$

In view of the boundary conditions Eq. (46), one obtains the following determinant equation for the load–frequency relationship of the nonlocal Eringen continuum (see [40]):

$$\begin{vmatrix} 1 & 0 & 1 & 0 \\ 0 & \widetilde{s}_1 & 0 & \widetilde{s}_2 \\ \left(\widetilde{s}_1^2 + \widetilde{r}\right)\cosh(\widetilde{s}_1) & \left(\widetilde{s}_1^2 + \widetilde{r}\right)\sinh(\widetilde{s}_1) & \left(-\widetilde{s}_2^2 + \widetilde{r}\right)\cos(\widetilde{s}_2) & \left(-\widetilde{s}_2^2 + \widetilde{r}\right)\sin(\widetilde{s}_2) \\ \left(\widetilde{s}_1^3 + \widetilde{s}_1\widetilde{r}\right)\sinh(\widetilde{s}_1) & \left(\widetilde{s}_1^3 + \widetilde{s}_1\widetilde{r}\right)\cosh(\widetilde{s}_1) & \left(\widetilde{s}_2^3 - \widetilde{s}_2\widetilde{r}\right)\sin(\widetilde{s}_2) & -\left(\widetilde{s}_2^3 - \widetilde{s}_2\widetilde{r}\right)\cos(\widetilde{s}_2) \end{vmatrix} = 0 \tag{48}$$

Equation (48) can be also presented equivalently as:

$$\widetilde{s}_1\widetilde{s}_2\left(\widetilde{s}_2^2 - \widetilde{r}\right)^2 + \widetilde{s}_1\widetilde{s}_2\left(\widetilde{s}_1^2 + \widetilde{r}\right)^2 + \left(\widetilde{s}_2^2 - \widetilde{s}_1^2\right)\left(\widetilde{s}_1^2 + \widetilde{r}\right)\left(\widetilde{s}_2^2 - \widetilde{r}\right)\sin(\widetilde{s}_2)\sinh(\widetilde{s}_1)$$
$$+ 2\widetilde{s}_1\widetilde{s}_2\left(\widetilde{s}_1^2 + \widetilde{r}\right)\left(\widetilde{s}_2^2 - \widetilde{r}\right)\cos(\widetilde{s}_2)\cosh(\widetilde{s}_1) = 0 \tag{49}$$

Figure 9 shows the load–frequency curve, $f(\Lambda, \Omega) = 0$, for $n = 4$, $n = 10$ and $n = 100$ in the domain of $\Lambda \in [0, 25]$, $\Omega \in [0, 25]$. The flutter load and flutter frequency parameters are: $\Lambda_{\text{flut}}^{\text{nonl},4} = 18.2148$ and $\Omega_{\text{flut}}^{\text{nonl},4} = 10.063$, respectively. The first natural frequency parameter is $\Omega_{\text{free}}^{\text{nonl},4} = 3.524$. For $n=10$, the flutter load and flutter frequency parameters in this case are: $\Lambda_{\text{flut}}^{\text{nonl},10} = 19.7335$ and $\Omega_{\text{flut}}^{\text{nonl},10} = 10.852$, respectively. The first free vibration frequency is $\Omega_{\text{free}}^{\text{nonl},10} = 3.517$. For $n = 100$, the flutter load and flutter frequency parameters are: $\Lambda_{\text{flut}}^{\text{nonl},100} = 20.0477$ and $\Omega_{\text{flut}}^{\text{nonl},100} = 11.014$, respectively. The first natural frequency parameter is $\Omega_{\text{free}}^{\text{nonl},100} = 3.516$.
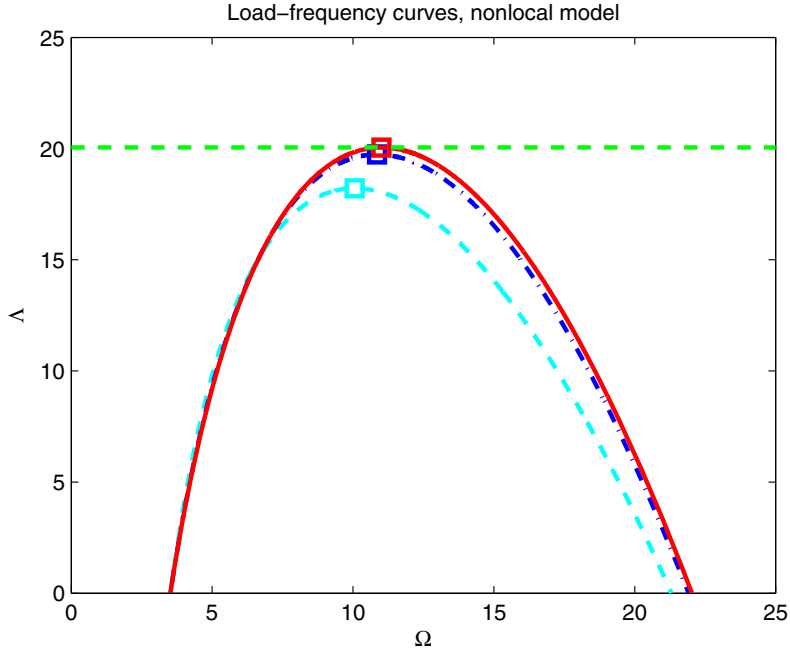
Fig. 9 Comparison of *load–frequency curve* of the nonlocal model for different values of *n*; $n = 4$ (*cyan dashed line*); $n = 10$ (*blue dash–dot line*); and $n = 100$ (*red solid line*). The flutter load–flutter frequency pair is denoted by a box. *Horizontal dashed line* shows Beck's flutter load; $l_c^2 = a^2/12$. (Color figure online)
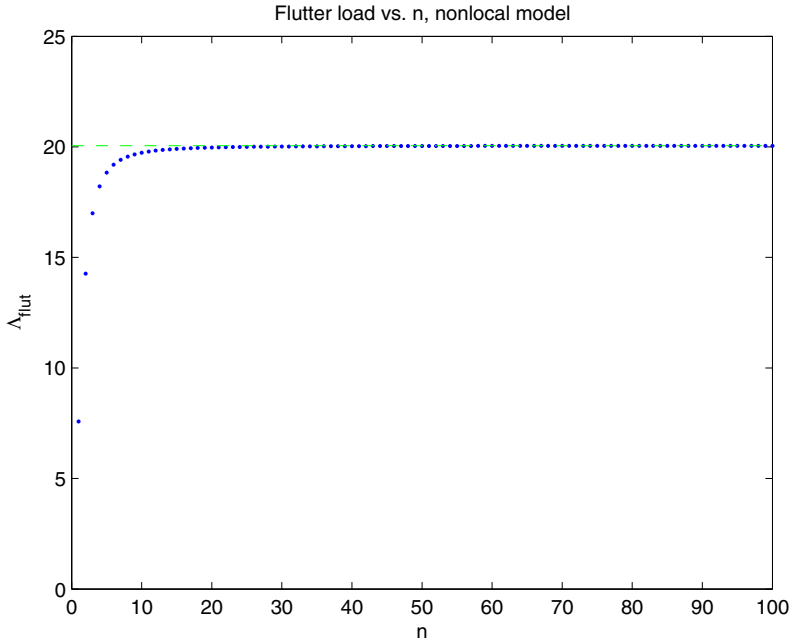

Fig. 10 Flutter load parameter of the nonlocal model versus *n*. *Dashed line* shows the flutter load of Beck's column; $l_c^2 = a^2/12$

Figure 10 shows the flutter load parameter versus *n* in the case of the nonlocal model, whereas Fig. 11 shows the flutter frequency parameter versus *n*. These results correspond to a fixed length scale, $l_c^2 = L^2/(12n^2)$.

Figure 12 shows the load–frequency curves of the discrete model, the continualized model with $l_c^2 = L^2/(12n^2)$, the nonlocal model with $l_c^2 = L^2/(12n^2)$ and the nonlocal model with $l_c^2 = L^2/(6n^2)$, for $n = 4$. These curves are shown for $n = 10$ in Fig. 13. All these results tend to Beck's solution as *n* is increased. Even if the softening microstructural effect is still observed here, the results are not as accurate for the Eringen's
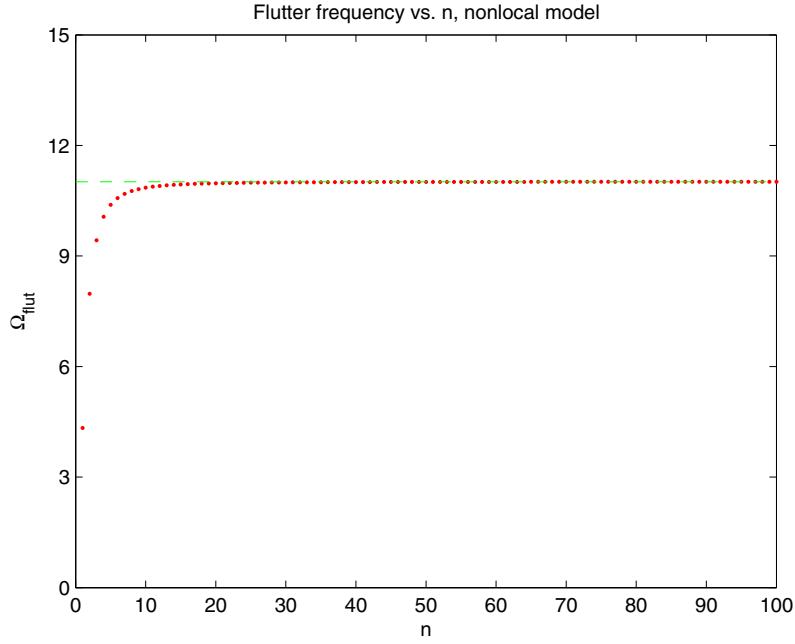
14

Fig. 11 Flutter frequency parameter of the nonlocal model versus n. *Dashed line* shows the flutter frequency of Beck's column; $l_c^2 = a^2/12$
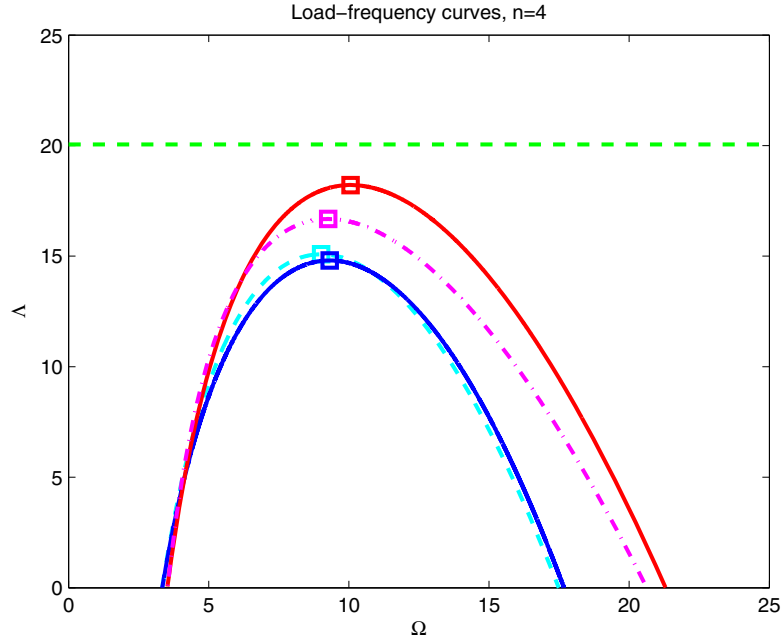

Fig. 12 *Load–frequency curves* of the discrete model (*cyan dashed line*), the continualized model with $l_c^2 = L^2/(12n^2)$ (*blue, solid internal line*), the nonlocal model with $l_c^2 = L^2/(12n^2)$ (*red, solid outer line*) and the nonlocal model with $l_c^2 = L^2/(6n^2)$ (*magenta dash-dot line*) with a fixed length scale, $n = 4$. (Color figure online)

nonlocal approach as for the continualized nonlocal model. In Figs. 14 and 15, the flutter load and the flutter frequency of the studied models are plotted as a function of n. Again, the results for the lattice and the nonlocal models are bounded below the results of the local continuum (local Beck's column—[6]). Surprisingly, the continualized nonlocal model is efficient in capturing the scale effect induced by the microstructure even for small values of n. Evolution of the fundamental natural frequency of the unloaded beam is plotted versus the
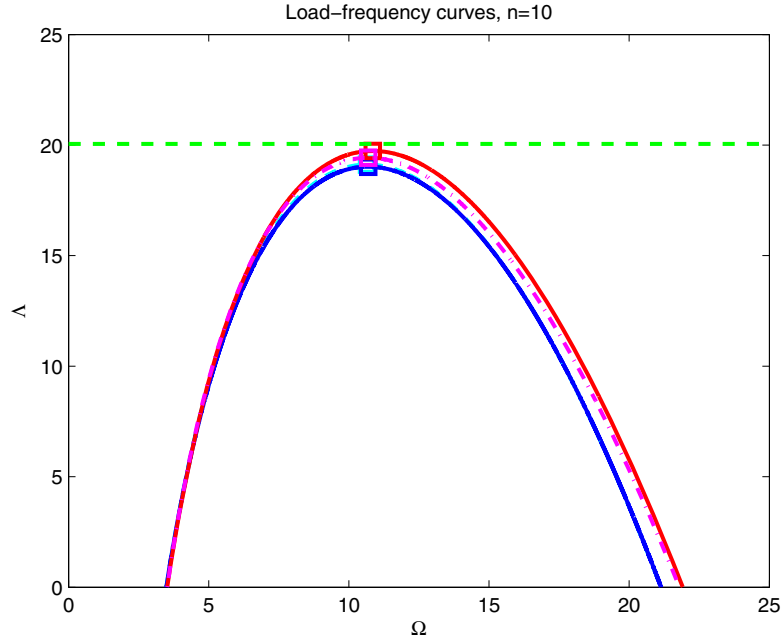
Fig. 13 *Load–frequency curves* of the discrete model (*cyan dashed line*), the continualized model with $l_c^2 = L^2/(12n^2)$ (*blue, solid internal line*), the nonlocal model with $l_c^2 = L^2/(12n^2)$ (*red, solid outer line*) and the nonlocal model with $l_c^2 = L^2/(6n^2)$ (*magenta dash-dot line*) with a fixed length scale, $n = 10$. (Color figure online)
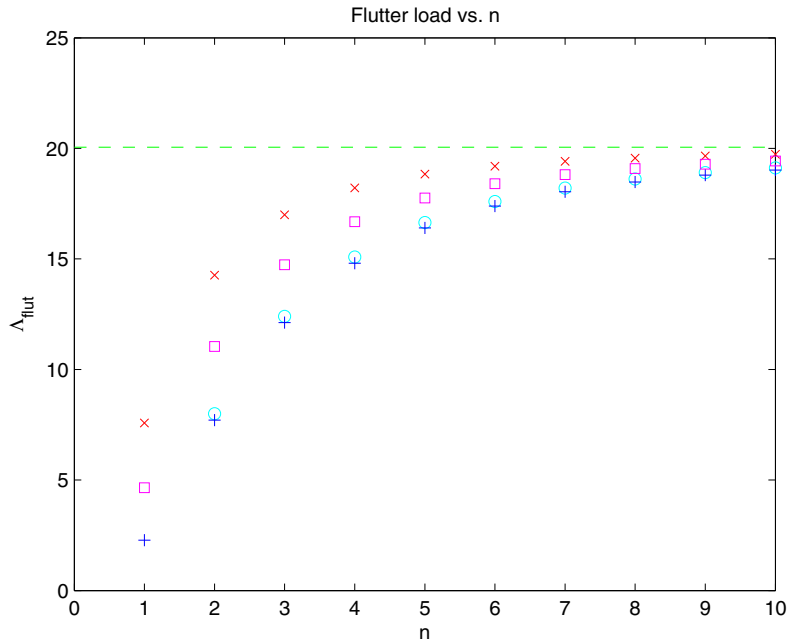

Fig. 14 Flutter load parameters of the discrete model (*cyan circle*), the continualized model with $l_c^2 = L^2/(12n^2)$ (*blue plus sign*), the nonlocal model with $l_c^2 = L^2/(12n^2)$ (*red cross*) and the nonlocal model with $l_c^2 = L^2/(6n^2)$ (*magenta square*) for various length scale n. *Dashed line* shows the flutter load of Beck's column. (Color figure online)

parameter n in Fig. 16. Again, the continualized nonlocal model is shown to fit perfectly the lattice model, whereas the (Eringen) nonlocal model presents some surprising small scale stiffening effect. As already analysed by [12], this stiffening effect can be removed from the consideration of a nonlocal-type boundary condition at the clamped section (or continualized nonlocal boundary conditions).
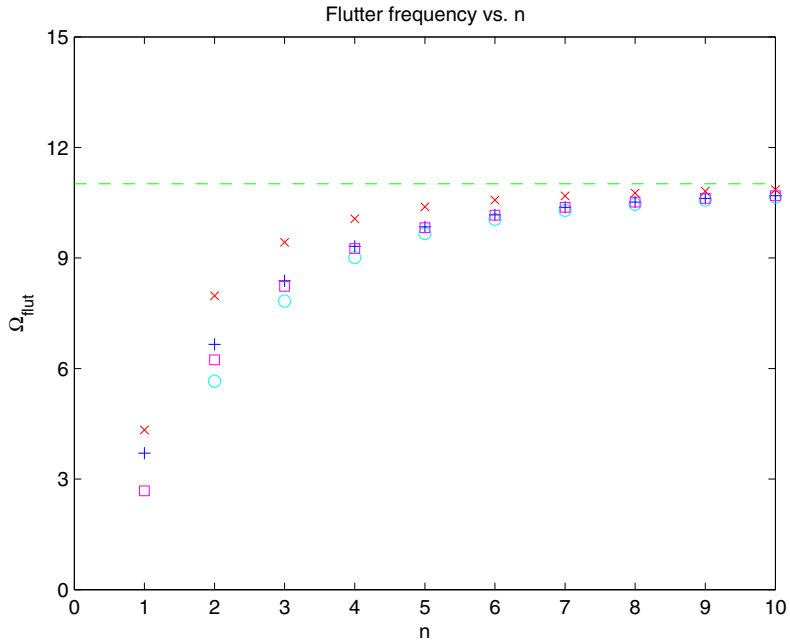
Fig. 15 Flutter frequency parameters of the discrete model (*cyan circle*), the continualized model with $l_c^2 = L^2/(12n^2)$ (*blue plus sign*), the nonlocal model with $l_c^2 = L^2/(12n^2)$ (*red cross*) and the nonlocal model with $l_c^2 = L^2/(6n^2)$ (*magenta square*) for various length scale n. *Dashed line* shows the flutter load of Beck's column. (Color figure online)
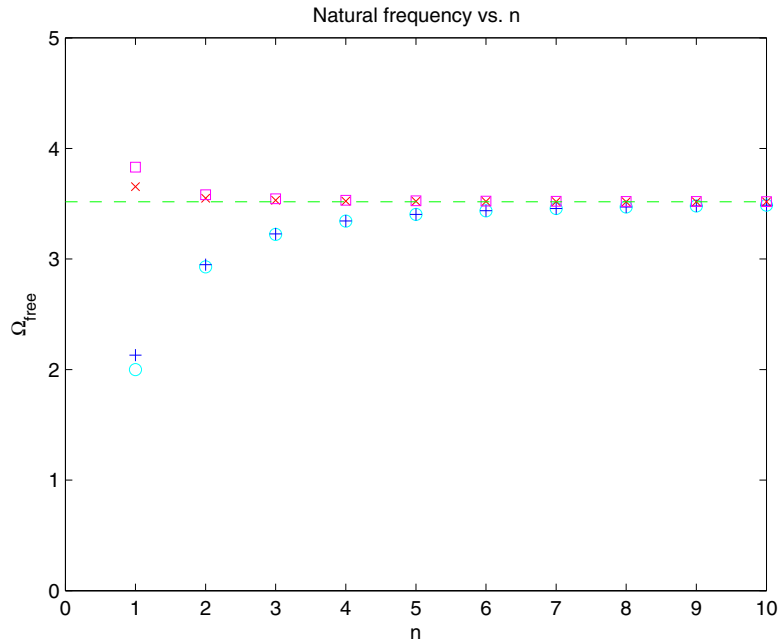

Fig. 16 First natural frequency parameters of the discrete model (*cyan circle*), the continualized model with $l_c^2 = L^2/(12n^2)$ (*blue plus sign*), the nonlocal model with $l_c^2 = L^2/(12n^2)$ (*red cross*) and the nonlocal model with $l_c^2 = L^2/(6n^2)$ (*magenta square*) for various length scale n. *Dashed line* shows the flutter load of Beck's column. (Color figure online)

Tables 1, 2 and 3 compare the flutter loads, the flutter frequencies and the first natural frequencies of the discrete model, the nonlocal model derived from continualization, and nonlocal model based on Eringen's approach with $l_c^2 = L^2/(12n^2)$ and $l_c^2 = L^2/(6n^2)$, for various values of n.

17

Table 1 Flutter loads of the discrete model (second row), the continualized model with $l_c^2 = L^2/(12n^2)$(third row), the nonlocal model with $l_c^2 = L^2/(12n^2)$(fourth row) and the nonlocal model with $l_c^2 = L^2/(6n^2)$ (fifth row) for various values of n

n	1	2	3	4	5	10	100	1000
$\Lambda_{\text{flut}}^{\text{disc}}$	–	8.0000	12.4023	15.0834	16.6458	19.1175	20.0413	20.0509
$\Lambda_{\text{flut}}^{\text{cont}}$	2.2781	7.7104	12.1184	14.8052	16.4026	19.0209	20.0402	20.0508
$\Lambda_{\text{flut}}^{\text{nonl}}$	7.5829	14.2615	16.9985	18.2148	18.8369	19.7335	20.0477	20.0509
$\Lambda_{\text{flut}}^{\text{nonl}}$	4.6541	11.0372	14.7374	16.6795	17.7579	19.4256	20.0445	20.0509

The flutter load of Beck's local column is $\Lambda_{\text{flut}}^{\text{Beck}} = 20.0510$

Table 2 Flutter frequencies of the discrete model (second row), the continualized model with $l_c^2 = L^2/(12n^2)$(third row), the nonlocal model with $l_c^2 = L^2/(12n^2)$(fourth row) and the nonlocal model with $l_c^2 = L^2/(6n^2)$ (fifth row) for various values of n

n	1	2	3	4	5	10	100	1000
$\Omega_{\text{flut}}^{\text{disc}}$	–	5.657	7.833	9.011	9.663	10.653	11.012	11.016
$\Omega_{\text{flut}}^{\text{cont}}$	3.703	6.654	8.382	9.316	9.846	10.689	11.012	11.016
$\Omega_{\text{flut}}^{\text{nonl}}$	4.331	7.976	9.426	10.063	10.387	10.852	11.014	11.016
$\Omega_{\text{flut}}^{\text{nonl}}$	2.683	6.236	8.230	9.259	9.825	10.692	11.012	11.016

The flutter frequency of Beck's local column is $\Omega_{\text{flut}}^{\text{Beck}} = 11.016$

Table 3 First natural frequencies of the discrete model (second row), the continualized model with $l_c^2 = L^2/(12n^2)$(third row), the nonlocal model with $l_c^2 = L^2/(12n^2)$(fourth row) and the nonlocal model with $l_c^2 = L^2/(6n^2)$ (fifth row) for various values of n

n	1	2	3	4	5	10	100	1000
$\Omega_{\text{free}}^{\text{disc}}$	2.000	2.928	3.221	3.342	3.402	3.487	3.516	3.516
$\Omega_{\text{free}}^{\text{cont}}$	2.129	2.948	3.226	3.344	3.403	3.487	3.516	3.516
$\Omega_{\text{free}}^{\text{nonl}}$	3.656	3.548	3.530	3.524	3.521	3.517	3.516	3.516
$\Omega_{\text{free}}^{\text{nonl}}$	3.835	3.582	3.545	3.532	3.526	3.519	3.516	3.516

The first natural frequency of Beck's local column is $\Omega_{\text{free}}^{\text{Beck}} = 3.516$

Finally, instead of using fixed length scales, $l_c^2 = L^2/(12n^2)$ or $l_c^2 = L^2/(6n^2)$, the following variable, load-dependent length scale parameter is implemented in the nonlocal model:

$$l_c^2 = \frac{L^2}{b \cdot n^2} \tag{50}$$

Here the value of b is calibrated such that the flutter load of the nonlocal model with a given n should fit the flutter load of the lattice model with the same n. Figure 17 shows the load–frequency curves of the discrete model and the nonlocal model with variable length scale parameter Eq. (50) for $n = 4$, $n = 10$ and $n = 100$. The value of b is plotted on the top of each diagram. It can be seen that for all the studied models, the discrete model, the nonlocal model obtained by continualization and the nonlocal model based on Eringen's approach are able to recover Beck's solution as $n \to \infty$. Note that n is the number of cells in the discrete problem, so $n \to \infty$ is the discrete to local continuum limit, while in the case of the nonlocal models, n is inversely proportional to the characteristic length of the material, and so $n \to \infty$ is the nonlocal continuum to the local continuum limit.

It has been shown that the continualized nonlocal model is superior to the phenomenological Eringen's nonlocal model. The reason is mainly due to the structure of equations of the lattice model (see also the discussion in Challamel et al. [12]), which can be presented as:

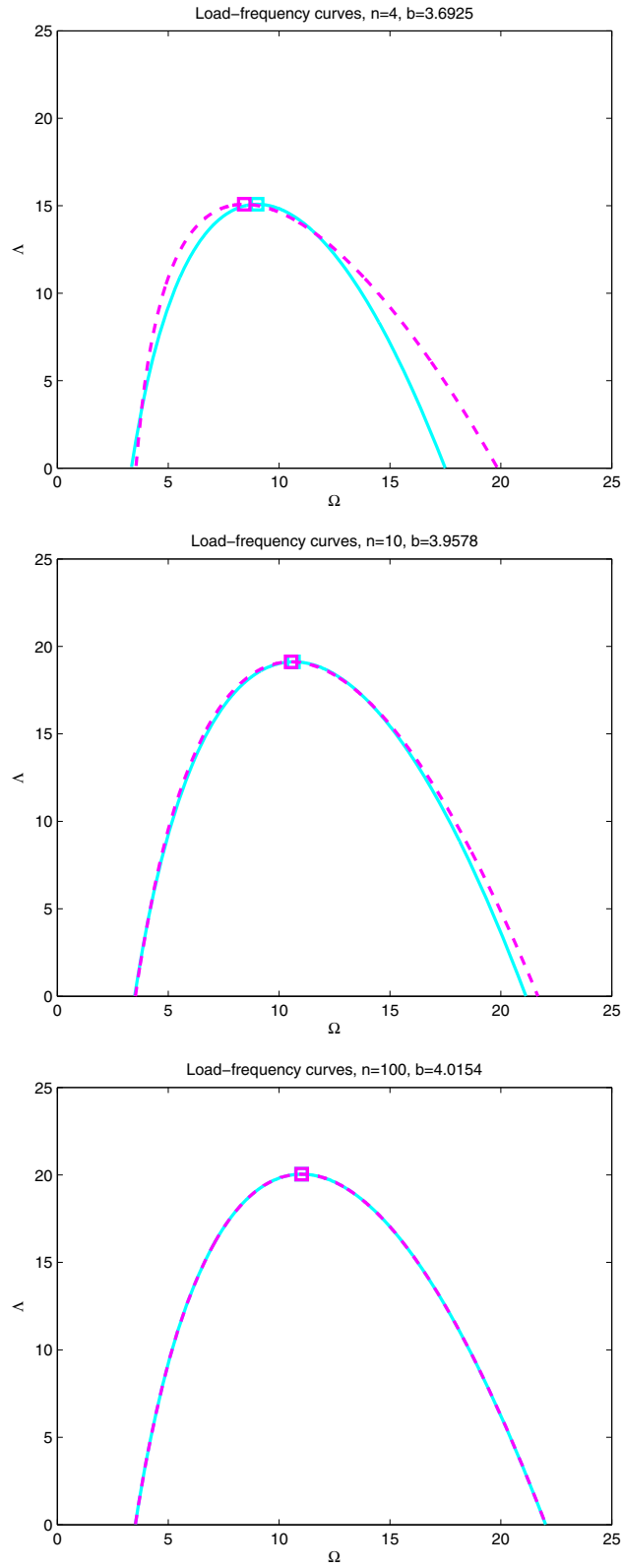$$M_i = EI\frac{w_{i-1} - 2w_i + w_{i+1}}{a^2} \tag{51a}$$

Fig. 17 Load–frequency curves of the discrete model (*cyan line*) and the nonlocal model with variable length scale parameter $l_c^2 = L^2/(b \cdot n^2)$ (*magenta dashed line*). (Color figure online)

and

$$\frac{M_{i-1} - 2M_i + M_{i+1}}{a^2} + P\frac{w_{i-1} - 2w_i + w_{i+1}}{a^2} + \mu\ddot{w}_i = 0 \tag{51b}$$

By applying the continualization procedure to both the constitutive law and the equilibrium equations, we obtain

$$M - l_c^2 M'' = EI\hat{w}'' \tag{52a}$$

and

$$M'' + P\hat{w}'' + \mu\left(\hat{\ddot{w}} - l_c^2\hat{\ddot{w}}''\right) = 0 \quad \text{with } l_c^2 = \frac{a^2}{12} \tag{52b}$$

It can be shown that Eq. (52) is equivalent to Eq. (32) if the terms in l_c^4 are neglected. In that respect, the continualized nonlocal model appears to be equivalent to Eringen's nonlocal model coupled with nonlocal equilibrium equations. In other words, both nonlocal models, the Eringen's one and the continualized nonlocal one, only differ by the possible nonlocal nature of the equilibrium equations (for comparable boundary conditions).

6 Conclusions

It has been shown that the discrete Beck's problem can be approximately studied using a nonlocal equivalent beam model produced from a continualization procedure. The discrete Beck column behaves as a nonlocal Beck column, where the nonlocality is found to depend on some length scale factor associated with the finite microstructure of the lattice. Two nonlocal models are considered, namely the Eringen stress gradient nonlocal model, which can be labelled as a phenomenological nonlocal model, and a continualized nonlocal model. The only difference between these two models lies in the equilibrium equations which remain local for the Eringen nonlocal model, whereas the continualized nonlocal model implicitly assumes a nonlocal effect both for the constitutive law and for the equilibrium equation (if comparable boundary conditions are chosen). These two nonlocal models both predict the softening behaviour of the microstructured Beck column when compared to the asymptotical local Beck problem. However, as anticipated, the continualized model furnishes closer results with respect to the reference lattice system. Nonlocal Beck's column is shown to be a transient medium from Ziegler's column (two-degree-of-freedom system) to the local continuous Beck's column (with an infinite degree of freedom). This paper confirms the capability of nonlocal beam mechanics to predict some scale effects in lattice bending systems, not only in the presence of conservative loadings, but also in the presence of nonconservative loadings.

Appendix 1

The flutter load of the two-degree-of-freedom Ziegler's type system (see Fig. 18) can be analytically obtained. The internal virtual work of this two-degree-of-freedom system is expressed from Eq. (9) as:

$$\delta W_{\text{int}} = 2C\theta_1\delta\theta_1 + C\left(\theta_1 - \theta_2\right)\left(\delta\theta_1 - \delta\theta_2\right) \tag{53}$$

The virtual work done by the follower force is:

$$\delta W_{\text{ext}} = Pa\left(\theta_1\delta\theta_1 + \theta_2\delta\theta_2\right) - Pa\theta_2\left(\delta\theta_1 + \delta\theta_2\right) = Pa\left(\theta_1 - \theta_2\right)\delta\theta_1 \tag{54}$$

The work done by the fictitious inertial force on a virtual displacement system is:

$$\delta W_f = -\frac{ma^2}{2}\left(\ddot{\theta}_1\delta\theta_1 + \ddot{\theta}_1\delta\theta_2 + \ddot{\theta}_2\delta\theta_1 + \ddot{\theta}_2\delta\theta_2\right) - ma^2\ddot{\theta}_1\delta\theta_1 \tag{55}$$
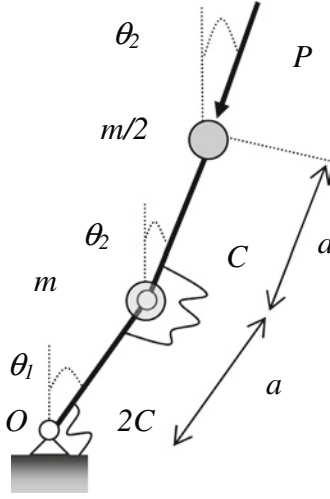
Fig. 18 Two-degree-of-freedom flutter system (Ziegler's type system)—$n = 2$

The total virtual work $\delta W = \delta W_{\text{int}} - \delta W_{\text{ext}} - \delta W_f$ is zero for *any* virtual displacement system, thus leading to the vibration equation:

$$\underline{\underline{M}}\,\ddot{\underline{\theta}} + \underline{\underline{K}}\,\underline{\theta} = \underline{0} \quad \text{with} \quad \underline{\underline{M}} = \frac{ma^2}{2}\begin{pmatrix} 3 & 1 \\ 1 & 1 \end{pmatrix}, \quad \underline{\underline{K}} = C\begin{pmatrix} 3 - \frac{Pa}{C} & -1 + \frac{Pa}{C} \\ -1 & 1 \end{pmatrix} \quad \text{and} \quad \underline{\theta} = \begin{pmatrix} \theta_1 \\ \theta_2 \end{pmatrix} \quad (56)$$

Note that $\underline{\underline{K}}$ is not symmetric as it also involves the effect of the nonconservative follower force. The circular frequency of the forced vibration is calculated from the determinant equation:

$$\det\left(\underline{\underline{K}} - \omega^2 \underline{\underline{M}}\right) = 0 \tag{57}$$

which can be equivalently presented using the dimensionless parameters:

$$\begin{vmatrix} 3 - \frac{\Lambda}{4} - \frac{3\Omega^2}{32} & -1 + \frac{\Lambda}{4} - \frac{\Omega^2}{32} \\ -1 - \frac{\Omega^2}{32} & 1 - \frac{\Omega^2}{32} \end{vmatrix} = 0 \quad \text{with} \quad \Lambda = \frac{PL^2}{EI} = n^2\frac{Pa}{C},$$

$$\Omega^2 = \frac{\omega^2 L^4}{EI}\mu = n^4\frac{\omega^2 a^2 m}{C} \quad \text{and} \quad n = 2 \tag{58}$$

The quartic frequency equation is obtained from the expansion of this determinant:

$$\Omega^4 + 8\Omega^2\left(\Lambda - 16\right) + 32^2 = 0 \tag{59}$$

The flutter frequency corresponds to the vanishing of the discriminant:

$$\Delta = 8^2\left(\Lambda - 16\right)^2 - 4 \times 32^2 = 0 \Rightarrow \Lambda = 8 \tag{60}$$

The flutter value $\Lambda_{\text{flut}}^{\text{disc},2} = 8$ is found for the two-degree-of-freedom Ziegler's type system $n = 2$. The flutter frequency is then obtained from Eq. (59) as:

$$\Omega_{\text{flut}}^{\text{disc},2} = 4\sqrt{2} \approx 5.657 \tag{61}$$

These values coincide with the numerical results, detailed in Tables 1 and 2. Note that Eq. (59) at $\Lambda = 0$ yields the nondimensional natural frequencies of the model. The first natural frequency is:

$$\Omega_{\text{free}}^{\text{disc},2} = \sqrt{64 - 32\sqrt{3}} \approx 2.928 \tag{62}$$

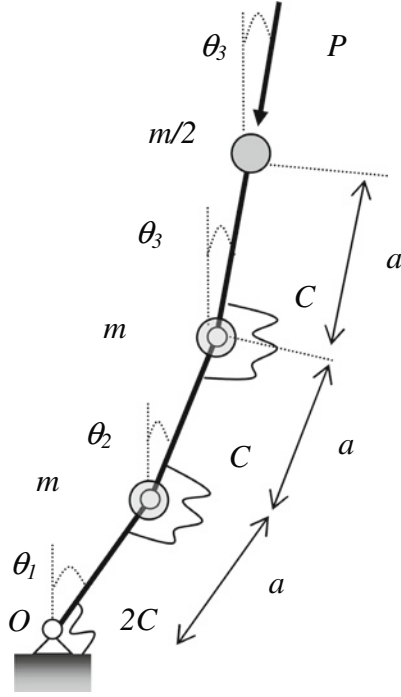It coincides with the corresponding value of Table 3.

Fig. 19 Three-degree-of-freedom flutter system—$n = 3$

Appendix 2

The flutter load of the three-degree-of-freedom follower load system (see Fig. 19) can be also analytically obtained. Following the reasoning already detailed in Appendix 1, and again considering that the total virtual work $\delta W = \delta W_{\text{int}} - \delta W_{\text{ext}} - \delta W_f$ is zero for *any* virtual displacement system, leads to the vibration equation:

$$\underline{\underline{M}}\,\underline{\ddot{\theta}} + \underline{\underline{K}}\,\underline{\theta} = \underline{0} \quad \text{with} \quad \underline{\underline{M}} = \frac{ma^2}{2}\begin{pmatrix} 5 & 3 & 1 \\ 3 & 3 & 1 \\ 1 & 1 & 1 \end{pmatrix},$$

$$\underline{\underline{K}} = C\begin{pmatrix} 3 - \frac{Pa}{C} & -1 & \frac{Pa}{C} \\ -1 & 2 - \frac{Pa}{C} & -1 + \frac{Pa}{C} \\ 0 & -1 & 1 \end{pmatrix} \quad \text{and} \quad \underline{\theta} = \begin{pmatrix} \theta_1 \\ \theta_2 \\ \theta_3 \end{pmatrix}$$

$$(63)$$

The circular frequency of the forced vibration is calculated from the determinant equation Eq. (57), which can be equivalently presented using the dimensionless parameters:

$$\det\left\{ \begin{pmatrix} 3 - \frac{\Lambda}{9} & -1 & \frac{\Lambda}{9} \\ -1 & 2 - \frac{\Lambda}{9} & -1 + \frac{\Lambda}{9} \\ 0 & -1 & 1 \end{pmatrix} - \frac{\Omega^2}{162}\begin{pmatrix} 5 & 3 & 1 \\ 3 & 3 & 1 \\ 1 & 1 & 1 \end{pmatrix} \right\} = 0 \quad \text{with}$$

$$\Lambda = n^2 \frac{Pa}{C} = 9\frac{Pa}{C}, \ \Omega^2 = n^4 \frac{\omega^2 a^2 m}{C} = 81\frac{\omega^2 a^2 m}{C} \quad \text{and} \quad n = 3 \qquad (64)$$

Now using the dimensionless variables $x = \Omega^2/(2n^4)$ and $p = \Lambda/n^2$, the determinant can be reformulated as:

$$\det\begin{pmatrix} 3 - p - 5x & -1 - 3x & p - x \\ -1 - 3x & 2 - p - 3x & -1 + p - x \\ -x & -1 - x & 1 - x \end{pmatrix} = 0 \qquad (65)$$

22

which is equivalently written by:

$$P(x) = 2 + \left(-33 + 20p - 3p^2\right)x + (28 - 8p)x^2 - 4x^3 \tag{66}$$

This cubic equation can be solved using Cardano's method. Put $y = x - \frac{1}{3}(7 - 2p)$, namely $x = y + \frac{1}{3}(7 - 2p)$, then x is a root of $P(x) = 0$ if and only if y is a root of $Q(y) = 0$, with $Q(y)$ defined by:

$$Q(y) = 719 - 498p + 123p^2 - 10p^3 + \left(873 - 468p + 63p^2\right)y - 108y^3 = -108\left(y^3 + vy + u\right)$$
$$\text{with} \quad u = \frac{719 - 498p + 123p^2 - 10p^3}{-108} \quad \text{and} \quad v = \frac{873 - 468p + 63p^2}{-108} \tag{67}$$

One recognizes the canonical form of the initial cubic equation (see Cardano's method). This cubic equation has multiple root when the discriminant of this cubic equation vanishes, i.e. when

$$\Delta = 4v^3 + 27u^2 = 0 \quad \Rightarrow 9p^6 - 192p^5 + 1702p^4 - 7984p^3 + 20725p^2 - 27840p + 14656 = 0 \tag{68}$$

This sixth-order polynomial equation can be numerically solved for the flutter load $p = \Lambda/n^2$. The first positive root of $\Delta(p) = 0$ is $p_f \approx 1.3780$, yielding the flutter load of the discrete model with n=3 cells:

$$\Lambda_{flut}^{disc,3} = 9 \times p_f \approx 12.4023 \tag{69}$$

which coincides with the corresponding result of Table 1.

When $\Delta(p) = 0$, the corresponding value of the flutter frequency $\Omega_{\text{flut}}^{\text{disc},3}$ is the double root of the cubic equation given by:

$$y_f = -\frac{3u}{2v} = \frac{-3\left(719 - 498p_f + 123p_f^2 - 10p_f^3\right)}{2\left(873 - 468p_f + 63p_f^2\right)} \Rightarrow x_f = -\frac{1}{2}\frac{-213 + 206p_f - 61p_f^2 + 6p_f^3}{97 - 52p_f + 7p_f^2} \tag{70}$$

One numerically finds $x_f \approx 0.378693$, which yields the flutter frequency of the discrete model with $n = 3$ cells:

$$\Omega_{\text{flut}}^{\text{disc},3} = 9\sqrt{2}\sqrt{x_f} \approx 7.833 \tag{71}$$

It coincides with the corresponding result of Table 2.

References

1. Andrianov, I.V., Awrejcewicz, J., Ivankov, O.: On an elastic dissipation model as continuous approximation for discrete media. Math. Probl. Eng. **27373**, 1–8 (2006)
2. Andrianov, I.V., Awrejcewicz, J., Weichert, D.: Improved continuous models for discrete media. Math. Probl. Eng. **986242**, 1–35 (2010)
3. Andrianov, I.V., Starushenko, G.A., Weichert, D.: Numerical investigation of 1D continuum dynamical models of discrete chain. Z. Angew. Math. Mech. **92**(11–12), 945–954 (2012)
4. Atanackovic, T.M., Bouras, Y., Zorica, D.: Nano and viscoelastic Beck's column on elastic foundation. Acta Mech. **226**(7), 2335–2345 (2015)
5. Awrejcewicz, J., Krysko, A.V., Zagniboroda, N.A., Dobriyan, V.V., Krysko, V.A.: On the general theory of chaotic dynamics of flexible curvilinear Euler–Bernoulli beams. Nonlinear Dyn. **79**, 11–29 (2015)
6. Beck, M.: Die Knicklast des einseitig eingespannten tangential gedrückten Stabes. Z. Angew. Math. Phys. **3**, 225–228 (1952)
7. Bolotin, V.V.: Nonconservative Problems of the Theory of Elastic Stability. Pergamon Press, New-York (1963)
8. Born, M., von Kármán, T.: On fluctuations in spatial grids. Physikalishe Zeitschrift **13**, 297–309 (1912)
9. Carr, J., Malhardeen, M.Z.M.: Beck's problem. SIAM J. Appl. Math. **37**(2), 261–262 (1979)
10. Challamel, N.: Variational formulation of gradient or/and nonlocal higher-order shear elasticity beams. Compos. Struct. **105**, 351–368 (2013)
11. Challamel, N., Lerbet, J., Wang, C.M., Zhang, Z.: Analytical length scale calibration of nonlocal continuum from a microstructured buckling model. Z. Angew. Math. Mech. **94**(5), 402–413 (2014a)
12. Challamel, N., Wang, C.M., Elishakoff, I.: Discrete systems behave as nonlocal structural elements: bending, buckling and vibration analysis. Eur. J. Mech. A/Solids **44**, 125–135 (2014b)

13. Challamel, N., Zhang, Z., Wang, C.M., Reddy, J.N., Wang, Q., Michelitsch, T., Collet, B.: On non-conservativeness of Eringen's nonlocal elasticity in beam mechanics: correction from a discrete-based approach. Arch. Appl. Mech. **84**(9), 1275–1292 (2014c)
14. Challamel, N., Kocsis, A., Wang, C.M.: Discrete and nonlocal elastica. Int. J. Non-linear Mech. **77**, 128–140 (2015a)
15. Challamel, N., Picandet, V., Collet, B., Michelitsch, T., Elishakoff, I., Wang, C.M.: Revisiting finite difference and finite element methods applied to structural mechanics within enriched continua. Eur. J. Mech. A/Solids **53**, 107–120 (2015b)
16. Duan, W.H., Challamel, N., Wang, C.M., Ding, Z.W.: Development of analytical vibration solutions for microstructured beam model to calibrate length scale coefficient in nonlocal Timoshenko beams. J. Appl. Phys. **114**(104312), 1–11 (2013)
17. El Naschie, M.S., Al-Athel, S.: Remarks on the stability of flexible rods under follower forces. J. Sound Vib. **64**, 462–465 (1979a)
18. El Naschie, M.S., Al-Athel, S.: On certain finite-element like methods for non-conservative sets. Solid Mech. Arch. **4**(3), 173–182 (1979b)
19. Elishakoff, I.: Controversy associated with the so-called "follower forces": critical overview. Appl. Mech. Rev. **58**(1–6), 117–142 (2005)
20. Eringen, A.C., Kim, B.S.: Relation between non-local elasticity and lattice dynamics. Crystal Lattice Defects **7**, 51–57 (1977)
21. Eringen, A.C.: On differential equations of nonlocal elasticity and solutions of screw dislocation and surface waves. J. Appl. Phys. **54**, 4703–4710 (1983)
22. Gantmacher, F.: Lectures in Analytical Mechanics. MIR Publishers, Moscow (1975)
23. Gasparini, A.M., Saetta, A.V., Vitaliani, R.V.: On the stability and instability regions of non-conservative continuous system under partially follower forces. Comput. Methods Appl. Mech. Eng. **124**, 63–78 (1995)
24. Hencky, H.: Über die angenäherte Lösung von Stabilitätsproblemen im Raummittels der elastischen Gelenkkette. Der Eisenbau **11**, 437–452 (1920). (in German)
25. Kocsis, A., Károlyi, G.: Conservative spatial chaos of buckled elastic linkages. Chaos **16**(033111), 1–7 (2006)
26. Kocsis, A.: An equilibrium method for the global computation of critical configurations of elastic linkages. Comput. Struct. **121**, 50–63 (2013)
27. Lazopoulos, K.A., Lazopoulos, A.K.: Stability of a gradient elastic beam compressed by non-conservative forces. Z. Angew. Math. Mech. **90**(3), 174–184 (2010)
28. Leckie, F.A., Lindberg, G.M.: The effect of lumped parameters on beam frequencies. Aeronaut. Quart. **14**(234), 224–240 (1963)
29. Leipholz, H.: Die Knicklast des einseitig eingespannten Stabes mit gleichmässig verteilter, tangentialer Längsbelastung. Z. Angew. Math. Mech. **13**, 581–589 (1962)
30. Leipholz, H.: Stability Theory. Academic Press, London (1970)
31. Luongo, A., D'Annibale, F.: On the destabilizing effect of damping on discrete and continuous circulatory systems. J. Sound Vib. **333**(24), 6723–6741 (2014)
32. Rosenau, P.: Dynamics of nonlinear mass-spring chains near the continuum limit. Phys. Lett. A **118**(5), 222–227 (1986)
33. Rosenau, P.: Dynamics of dense lattices. Phys. Rev. B **36**(11), 5868–5876 (1987)
34. Santoro, R., Elishakoff, I.: Accuracy of the finite difference method in stochastic setting. J. Sound Vib. **291**(1–2), 275–284 (2006)
35. Silverman, I.K.: Discussion on the paper of "Salvadori M.G., Numerical computation of buckling loads by finite differences". Trans. ASCE **116**, 590–636 (1951). Trans. ASCE **116**, 625–626 (1951)
36. Sugiyama, Y., Fujiwara, N., Sekiya, T.: Studies on nonconservative problems of instabilities of columns by means of Analog computer. Trans. Jpn. Soc. Mech. Eng. **37**(297), 931–940 (1971). (in Japanese)
37. Sugiyama, Y., Kawagoe, H.: Vibration and stability of elastic columns under the combined action of uniformly distributed vertical and tangential forces. J. Sound Vib. **38**(3), 341–355 (1975)
38. Wang, C.M., Zhang, Z., Challamel, N., Duan, W.H.: Calibration of Eringen's small length scale coefficient for initially stressed vibrating nonlocal Euler beams based on microstructured beam model. J. Phys. D Appl. Phys. **46**, 345501 (2013)
39. Wattis, J.A.D.: Quasi-continuum approximations to lattice equations arising from the discrete non-linear telegraph equation. J. Phys. A Math. Gen. **33**, 5925–5944 (2000)
40. Xiang, Y., Wang, C.M., Kitipornchai, S., Wang, Q.: Dynamic instability of nanorods/nanotubes subjected to an end follower force. J. Eng. Mech. **136**, 1054–1058 (2010)
41. Zhang, Z., Challamel, N., Wang, C.M.: Eringen's small length scale coefficient for buckling of nonlocal Timoshenko beam based on a microstructured beam model. J. Appl. Phys. **114**(114902), 1–6 (2013)
42. Zhang, Z., Wang, C.M., Challamel, N., Elishakoff, I.: Obtaining Eringen's length scale coefficient for vibrating nonlocal beams via continualization method. J. Sound Vib. **333**, 4977–4990 (2014)
43. Ziegler, H.: Die Stabilitätskriterien der Elastomechanik. Ingenieur-Archiv **20**, 49–56 (1952)
44. Ziegler, H.: Principles of Structural Stability. Blaisdell Publishing Co, Waltham (1968)